Dependence of quantum-Hall conductance on the edge-state equilibration position in a bipolar graphene sheet

Dong-Keun Ki,[1] Seung-Geol Nam,[1] Hu-Jong Lee,[1,2,*] and Barbaros Özyilmaz[3]

[1]*Department of Physics, Pohang University of Science and Technology, Pohang 790-784, Republic of Korea*
[2]*National Center for Nanomaterials Technology, Pohang 790-784, Republic of Korea*
[3]*Department of Physics, National University of Singapore, Singapore 117542, Singapore*

By using four-terminal configurations, we investigated the dependence of longitudinal and diagonal resistances of a graphene p-n interface on the quantum-Hall edge-state equilibration position. The resistance of a p-n device in our four-terminal scheme is asymmetric with respect to the zero point where the filling factor (ν) of the entire graphene vanishes. This resistance asymmetry is caused by the chiral direction dependent change in the equilibration position and leads to a deeper insight into the equilibration process of the quantum-Hall edge-states in a bipolar graphene system.

Half-integer quantum-Hall (QH) effect in graphene manifests the massless Dirac-fermionic nature of carriers in the material.[1,2] The corresponding QH edge-state in graphene has been explicitly confirmed to be chiral[3] as in an ordinary two-dimensional (2D) electron gas.[4–6] Since carriers in graphene possess bipolar characteristics, the filling factor (ν) and the chiral direction of the edge-states can be modulated by gating a graphene sheet electrostatically.[1,2] Although the spatial deflection of an edge-state is hard to be realized,[7] a partial reflection of the edge-state can be accomplished in locally gated graphene devices by means of the edge-state equilibration at p-n interfaces.[8–11] Nonetheless, previous conductance measurements, either in two-terminal[8–10] or in four-terminal configurations,[11] did not explicitly reveal the dependence of the conductance on the equilibration position (EP), where the edge-states with different filling factors are equilibrated.

Recently, by measuring four-terminal magnetoresistance of a spatially chemical-doped graphene p-n device, the longitudinal resistances are shown to be either quantized at finite values or vanish depending on the gate voltage, the measurement configuration, and the magnetic field (H) direction.[12] Analysis of the data confirmed that the four-terminal magnetoresistance depends on the location of the EP. From this result, one may suppose that the location of the EP can be experimentally determined simply by measuring four-terminal longitudinal magnetoresistance in any hybrid systems. In the study, however, the ν of the chemically doped region was not flexibly controllable, as distinct from the locally top-gated devices, where the ν of the top-gated region can be controlled separately from the region of the global gating only. In this study, we took the longitudinal (R_L) and the diagonal (R_D) resistances of a graphene p-n interface established by a local top-gate in four-terminal configurations. The measurement scheme enabled us to access in detail the development of the equilibration condition of the QH edge conducting states in graphene. We locate the EP's corresponding to different measurement configurations and explicitly show that both four-terminal R_L and R_D are sensitive to the location of the EP.

A graphene p-n device was fabricated by electron-beam

patterning and depositing a Cr (5 nm)/Au (25 nm) bilayer on a mechanically exfoliated monolayer graphene sheet.[13] It was then followed by the polymethyl methacrylate (PMMA; 950 K, 2% in anisole) insulation[14] and the deposition of a local gate, which covered one side of the sample[11] [Figs. 1(a) and 1(b)]. The device was cooled down to 120 mK in a dilution fridge and $R_D(=V_D/I)$ and $R_L(=V_L/I)$ were obtained in two different measurement configurations [Figs. 1(c) and 1(d)] by using the conventional lock-in technique.[11] The bipolar character of the device was verified at zero magnetic field H by measuring R_L as a function of local-gate and back-gate voltages (V_{LG} and V_{BG}, respectively), which exhibits a crosslike structure in the parameter space set up by the local variation in the density and the type of conduction carriers[11] (not shown).
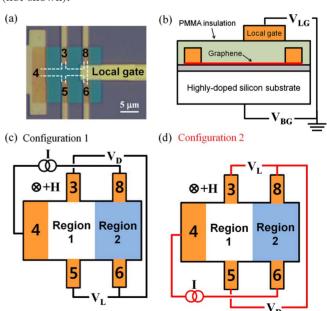

FIG. 1. (Color online) (a) Optical image of the sample. A PMMA insulation layer covers the graphene sheet, the boundary of which is defined by white broken lines. The white scale bar represents 5 μm. (b) Schematic gate configuration. (c) Measurement configuration 1. (d) Measurement configuration 2.
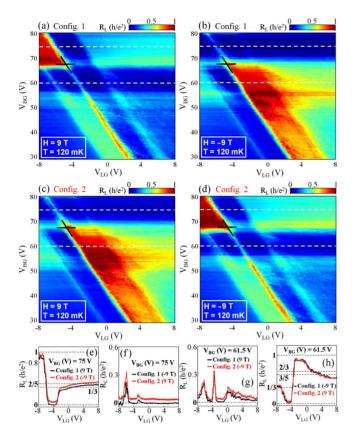
FIG. 2. (Color online) (a) and (b) 2D contrast maps of $R_L(V_{LG}, V_{BG})$ for the configuration 1, and $H=9$ T and -9 T, respectively. (c) and (d) 2D contrast maps of $R_L(V_{LG}, V_{BG})$ for the configuration 2, and $H=9$ T and -9 T, respectively. White broken lines in (a)–(d) indicate the values of V_{BG} where the slice data in (e)–(h) are extracted. (e) and (f) Slice plots of 2D contrast maps at $V_{BG}=75$ V. (g)–(h) Slice plots of 2D contrast maps at $V_{BG}=61.5$ V. Black and gray lines in (e)–(h) represent the slice data for the configurations 1 and 2, respectively.

The 2D contrast maps in Fig. 2 display $R_L(V_{LG}, V_{BG})$ measured in two different configurations at $H=\pm 9$ T. Figures 2(a)–2(d) have several skewed blocks with varied contrast, i.e., with differently quantized resistances. Each figure has an asymmetry with respect to the zero point (a black cross), where the value of ν of the QH edge-states in the regions $1(\nu_1)$ and $2(\nu_2)$ vanishes. The region 1 (2) represents the area outside (underneath) the local gate [Figs. 1(c) and 1(d)]. Figure 2(a), which corresponds to the configuration 1 and $H=+9$ T, is analogous to Fig. 2(d) for the configuration 2 and $H=-9$ T. Similarly, Fig. 2(b) nearly duplicates Fig. 2(c). On the other hand, resistances for opposite configurations at a given H [Figs. 2(a) and 2(b) or Figs. 2(c) and 2(d)] have 180°-rotational symmetry with respect to the zero point. This is in contrast to earlier two-terminal studies, where conductances were always symmetric,[8,10] as well as to the four-terminal studies on a p-n-p device, where only R_D exhibited an asymmetry.[11]

Details of resistance variations can be analyzed by examining slices of Figs. 2(a)–2(d) at two different values of V_{BG}, as shown in Figs. 2(e)–2(h). Each figure contains two such slices black and gray lines for a concurrent change of the measurement configuration and the H direction. As expected,
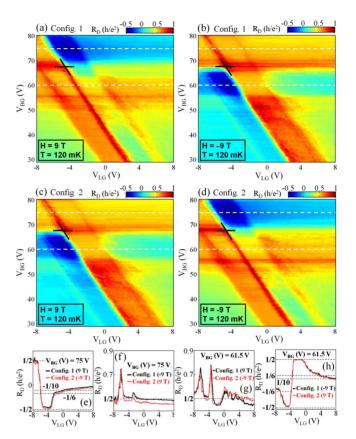
FIG. 3. (Color online) (a)–(b) 2D contrast maps of $R_D(V_{LG}, V_{BG})$ for the configuration 1, and $H=9$ T and -9 T, respectively. (c)–(d) 2D contrast maps of $R_D(V_{LG}, V_{BG})$ for the configuration 2, and $H=9$ T and -9 T, respectively. White broken lines in (a)–(d) indicate the values of V_{BG} where slice data in (e-h) are extracted. (e) and (f) Slice plots of 2D contrast maps at $V_{BG}=75$ V. (g) and (h) Slice plots of 2D contrast maps at $V_{BG}=61.5$ V. Black and gray lines in (e-h) represent the slice data for the configurations 1 and 2, respectively.

black and gray lines in each slice are almost identical. R_L's in Figs. 2(f) and 2(g) oscillate with zero resistance plateaus, which are the Shubnikov-de Hass oscillations in the region 2. However, R_L's in Figs. 2(e) and 2(h) show a few plateaus, some with fractional resistances. This is an indication of the finite edge-state reflection at the p-n interface.[11] One notes that the difference between Fig. 2(e) [Fig. 2(h)] and Fig. 2(f) [Fig. 2(g)], which are in an identical configuration, is in the H direction only. It will be shown below that this seeming strange feature arises from the sensitivity of a four-terminal resistance on the location of the EP in our graphene p-n device.

We also measured $R_D(V_{LG}, V_{BG})$ as plotted in Fig. 3. Similar to the behavior of Figs. 2(a)–2(d), Fig. 3(a) [Fig. 3(b)] resembles Fig. 3(d) [Fig. 3(c)] but with an inversion symmetry with Fig. 3(c) [Fig. 3(d)]. Each slice plot in Figs. 3(e)–3(h) and the corresponding one in Figs. 2(e)–2(h) are qualitatively similar despite some quantitative differences. Moreover, in Figs. 3(e)–3(h), one can see that R_D is always the Hall resistance either for the region $1(R_{H1})$ or for the region $2(R_{H2})$. It is easily explained by the Kirchhoff's current-conservation relation, which points out that R_D is the
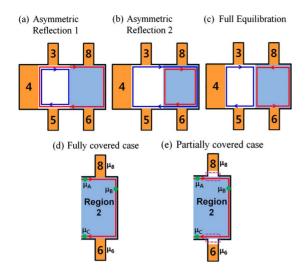
FIG. 4. (Color online) Schematic configurations of the edge-state circulation for (a) the asymmetric reflection 1, (b) the asymmetric reflection 2, and (c) the full equilibration. The configuration with the local gate (d) fully covering and (e) partially covering the area between leads 6 and 8.

summation of R_{H1} or R_{H2} and the corresponding R_L. Consequently, symmetries imposed upon R_L should appear in R_D.

Transport properties of the QH edge-state can be conveniently analyzed by the Landauer-Büttiker formula.[5,6,11] Based on the complete-mode-mixing hypothesis,[9,11] one can distinguish three equilibration regimes: the asymmetric reflection 1 ($\nu_1 \cdot \nu_2 > 0$ and $|\nu_1| \geq |\nu_2|$), the asymmetric reflection 2 ($\nu_1 \cdot \nu_2 > 0$ and $|\nu_1| < |\nu_2|$), and the full equilibration ($\nu_1 \cdot \nu_2 < 0$) regimes. Figures 4(a)–4(c) illustrate the schematics of the edge-state circulation in each regime for $\nu_1 < 0$ and $+H$. The asymmetric reflection 1 [Fig. 4(a)] is the case where the edge-states inside the region 2 are not reflected at the interface. The situation is opposite for the asymmetric reflection 2 [Fig. 4(b)]. In full equilibration regime [Fig. 4(c)], the edge-states in the regions 1 and 2 merge at the one side of the sample [for example, the upper side in Fig. 4(c)] and split at the other side [the lower side in Fig. 4(c)].

By evaluating scattering matrices, we calculated R_L and R_D as a function of ν_1 and ν_2 for different measurement conditions and equilibration regimes.[5,6,11] Detailed results are summarized below for $\nu_1 < 0$ and $+H$.

(a) Asymmetric reflection 1($\nu_1 \cdot \nu_2 > 0, |\nu_1| \geq |\nu_2|$)

$$R_D = \begin{cases} \dfrac{h}{e^2}\dfrac{1}{|\nu_2|} & \text{(Configuration 1)} \\[2ex] -\dfrac{h}{e^2}\dfrac{1}{|\nu_1|} & \text{(Configuration 2)} \end{cases},$$

$$R_L = \begin{cases} \dfrac{h}{e^2}\dfrac{|\nu_1|-|\nu_2|}{|\nu_1||\nu_2|} & \text{(Configuration 1)} \\[2ex] 0 & \text{(Configuration 2)} \end{cases}. \quad (1)$$

(b) Asymmetric reflection 2($\nu_1 \cdot \nu_2 > 0, |\nu_1| < |\nu_2|$)

$$R_D = \begin{cases} \dfrac{h}{e^2}\dfrac{1}{|\nu_1|} & \text{(Configuration 1)} \\[2ex] -\dfrac{h}{e^2}\dfrac{1}{|\nu_2|} & \text{(Configuration 2)} \end{cases},$$

$$R_L = \begin{cases} 0 & \text{(Configuration 1)} \\[2ex] \dfrac{h}{e^2}\dfrac{|\nu_2|-|\nu_1|}{|\nu_1||\nu_2|} & \text{(Configuration 2)} \end{cases}. \quad (2)$$

(c) Full equilibration ($\nu_1 \cdot \nu_2 < 0$)

$$R_D = \begin{cases} \dfrac{h}{e^2}\dfrac{1}{|\nu_1|} & \text{(Configuration 1)} \\[2ex] \dfrac{h}{e^2}\dfrac{1}{|\nu_2|} & \text{(Configuration 2)} \end{cases},$$

$$R_L = \begin{cases} 0 & \text{(Configuration 1)} \\[2ex] \dfrac{h}{e^2}\dfrac{|\nu_1|+|\nu_2|}{|\nu_1||\nu_2|} & \text{(Configuration 2)} \end{cases}. \quad (3)$$

In Eq. (1), R_L for the configuration 2($=V_{38}/I$) vanishes but it is finite in Eqs. (2) and (3), which is in coincidence with our experimental findings [compare Fig. 2(a) with Fig. 2(b) for $V_{BG} < \sim 55$ V]. Here, $V_{\alpha\beta}$ stands for the voltage difference between the leads α and β. The behavior of R_L results because the EP in the asymmetric reflection 1 regime is different from that in the other regimes. In the former regime, the edge-states are equilibrated at the lower boundary of the sample between the leads 5 and 6 [Fig. 4(a)], so that V_L (or equivalently R_L) for the configuration 1($=V_{56}$) is finite while the one for the configuration 2($=V_{38}$) vanishes. On the contrary, in the asymmetric reflection 2 [Figs. 4(b)] and the full equilibration [Figs. 4(c)] cases, the equilibration takes place at the upper boundary of the sample between the leads 3 and 8, resulting in the finite R_L in the configuration 2($=V_{38}/I$). Since the EP depends on the chiral direction of the edge-state circulation, R_L in the configuration 1 (2) for $\nu_1 < 0$ becomes identical to the one in the configuration 2 (1) for $\nu_1 > 0$ for an identical H. Equivalently, R_L for $\nu_1 < 0$ in a negative H becomes the same as that for $\nu_1 > 0$ in a positive H. It agrees with symmetries found in our experiment [Fig. 2]. Moreover, as shown as broken lines in Figs. 2(e)–2(h), calculations and experiments are in a quantitative agreement with each other. It is important to point out that, in a p-n-p device, the EP's at opposite sides of the local-gate are located at different (upper or lower) boundaries of the sample. Thus, four-terminal R_L of a graphene p-n-p device does not reveal the dependence on the location of EP, although the EP itself sensitively depends on the chiral direction of the QH edge-state.[11]

The calculated R_D also coincides with the experimental value [Fig. 3], which is always R_{H1} or R_{H2}. This can be explained by a simple Kirchhoff's law. For instance, V_{36} is the summation of V_{38} and $V_{86}(=R_{H2} \times I)$ or equally V_{35} ($=R_{H1} \times I$) and V_{56}. As V_{38} is zero in the asymmetric reflection 1 regime, R_D for the configuration 1($=V_{36}/I$) will be R_{H2} [Eq. (1)]. For the same reason, V_{58}/I ($=R_D$ for the configuration 2) should be $-R_{H1}$ [Eq. (1)]. In the other regimes, V_{56}

vanishes [Eqs. (2) and (3)], so that R_D becomes R_{H1} for the configuration 1 and $-R_{H2}$ for the configuration 2.

Up to this point, we consider only the cases where all the regions between the leads 6 and 8 are covered by local gates [Fig. 4(d)]. However, as seen in Fig. 4(e), the regions near the leads 6 and 8 may not be fully covered by the local gates, which results in the formation of unintended p-n interfaces around the regions [dotted squares in Fig. 4(e)]. This may change the conductance features we discuss above. Apparently, the conductance change takes place in a two-terminal configuration as the additional interface forms a p-n-p junction between the source and the drain. But, in the following discussion, we demonstrate that the results of four-terminal measurements are not affected. This implies that the difference in the chemical potential (μ) between the point A and the lead 6 ($\mu_A - \mu_6$) remains the same for both fully and partially covered cases, when the leads 6 and 8 are a voltage probe and a drain, respectively [here, we focus on the configuration 1 in Fig. 1(c) but the same argument is valid for the configuration 2]. As the chemical potential does not change across the voltage probe without current flow, it is straightforward to show that μ_6 is always identical to μ_B and μ_C for both cases. In addition, the Hall voltage inside the region 2, $\mu_A - \mu_B$, does not vary irrespective of the presence or the absence of p-n interfaces outside the region 2 (the region covered by the local gate). Consequently, the presence of additional bipolar interfaces does not affect the value $\mu_A - \mu_6$, neither the corresponding four-terminal resistances. One note that for the partially covered case μ_B can differ from μ_8 in certain equilibration regimes so that the partial coverage of the top gate affects the two-terminal results. This demonstrates the high benefit of the multiterminal measurements in comparison with the two-terminal ones for edge-state equilibration studies.

In this study, we independently controlled the local filling factors of the top gated and the rest of back-gated region of a graphene sheet. It enabled us to access to diverse combination of bipolar configurations in the sheet along with more systematic examination of equilibration condition of QH edge conducting states. We have shown that both the longitudinal (R_L in Fig. 2) and the diagonal (R_D in Fig. 3) resistances, obtained in four-terminal configurations, of this *locally top-gated* hybrid p-n junction device are asymmetric with respect to the zero point. The behaviors of R_L and R_D are also in clear contrast to the two-terminal studies on *locally top-gated p-n* (Ref. 8) and *p-n-p* (Ref. 10) devices of graphene as well as to similar four-terminal studies on *locally top-gated p-n-p* devices.[11] The resistances in two different measurement configurations [Figs. 1(c) and 1(d)] and H directions confirms that the asymmetry is caused by the dependence of the four-terminal resistance of a graphene p-n interface on the location of the EP, which varies with the chiral direction of the QH edge-state. Since two-terminal conductances do not depend on the chiral direction and the EP's in a p-n-p device are always located at opposite boundaries of the sample, the location of the EP could not be traced in the previous experiments and the resistances turned out to be symmetric.[8,10,11] This four-terminal study on a graphene p-n interface provides a deeper insight into how and where the QH edge-states are equilibrated in a locally gated graphene system, which is essential in designing devices such as quantum interferometers out of graphene.

*Corresponding author; hjlee@postech.ac.kr

[1] K. S. Novoselov, A. K. Geim, S. V. Morozov, D. Jiang, M. I. Katsnelson, I. V. Grigorieva, S. V. Dubonos, and A. A. Firsov, Nature (London) **438**, 197 (2005).

[2] Y. Zhang, Y. W. Tan, H. L. Stormer, and P. Kim, Nature (London) **438**, 201 (2005).

[3] D. K. Ki, S. Jo, and H. J. Lee, Appl. Phys. Lett. **94**, 162113 (2009).

[4] B. I. Halperin, Phys. Rev. B **25**, 2185 (1982).

[5] M. Büttiker, Phys. Rev. B **38**, 9375 (1988).

[6] See a review in C. W. J. Beenakker and H. van Houten, Solid State Phys. **44**, 1 (1991), arXiv:cond-mat/0412664.

[7] M. I. Katsnelson, K. S. Novoselov, and A. K. Geim, Nat. Phys. **2**, 620 (2006).

[8] J. R. Williams, L. DiCarlo, and C. M. Marcus, Science **317**, 638 (2007).

[9] D. A. Abanin and L. S. Levitov, Science **317**, 641 (2007).

[10] B. Özyilmaz, P. Jarillo-Herrero, D. Efetov, D. A. Abanin, L. S. Levitov, and P. Kim, Phys. Rev. Lett. **99**, 166804 (2007).

[11] D. K. Ki and H. J. Lee, Phys. Rev. B **79**, 195327 (2009).

[12] T. Lohmann, K. v. Klitzing, and J. H. Smet, Nano Lett. **9**, 1973 (2009).

[13] K. S. Novoselov, A. K. Geim, S. V. Morozov, D. Jiang, Y. Zhang, S. V. Dubonos, I. V. Grigorieva, and A. A. Firsov, Science **306**, 666 (2004).

[14] B. Huard, J. A. Sulpizio, N. Stander, K. Todd, B. Yang, and D. Goldhaber-Gordon, Phys. Rev. Lett. **98**, 236803 (2007).